Cancer Imaging

DOI: 10.1002/anie.201104507

X-Ray Computed Tomography Imaging of Breast Cancer by using Targeted Peptide-Labeled Bismuth Sulfide Nanoparticles**

*Joseph M. Kinsella, Rebecca E. Jimenez, Priya P. Karmali, Anthony M. Rush, V. Ramana Kotamraju, Nathan C. Gianneschi, Erkki Ruoslahti, Dwayne Stupack, and Michael J. Sailor**

Tissue-specific nanoparticles have shown great potential as contrast agents for in vivo medical imaging of several cancer types.[1–3] Much of the work thus far has focused on nanoparticle contrast agents for magnetic resonance and optical imaging studies.[4–8] More recently, X-ray computed tomography (CT) probes based on iodine, gold, and bismuth nanomaterials have been demonstrated in vivo.[6,9–12] Bi_2S_3 nanoparticles are well-suited as CT contrast agents owing to the large atomic number of Bi ($z = 83$) compared to currently available clinical or pre-clinical alternatives, such as iodinated ($z = 53$) or gold-based systems ($z = 79$),[12–14] and nanoparticles of Bi_2S_3 have been shown to be equal or superior to iodinated CT contrast agents.[12] Here we present the synthesis and in vivo characterization of bismuth sulfide (Bi_2S_3) nanoparticles labeled with the cyclic nine amino acid peptide, CGNKRTRGC (LyP-1)-targeted to 4T1 breast cancer in mice. The molecular signature of the cells, lymphatics, and vessels associated with tumors often differ from healthy tissues, and molecules such as Lyp-1 can specifically bind to these features to deliver contrast agents in a site-specific manner.[15–20] The nanoparticles showed limited signs of acute cytotoxicity at concentrations up to 0.03 M Bi, and the LyP-1 peptide-labeled nanoparticles preferentially accumulated into 4T1 tumors both in vitro and in vivo, enabling acquisition of high fidelity CT images of the orthotopic tumor, particularly at the tumor margins.

The homing peptide used in this study, LyP-1, was previously isolated from a screen using MDA-MB-435 human cancer xenografts.[21] This was the first peptide that showed specific homing to tumor lymphatic vessels in addition to other cells in tumor tissues. The ability of species labeled with LyP-1 to target tumor-draining lymph nodes was confirmed by blocking experiments, in which targeting was observed in the presence of free LyP-1.[22] The cellular receptor for LyP-1 is the gC1q receptor p32 protein.[23] Elevated levels of this protein have been detected in a variety of tumor cell lines, in addition to clinical samples of human carcinoma.[23] The tumor cell lines used in this study, 4T1 mouse breast cancer cells, are known to overexpress the p32 protein on their cell and mitochondrial membranes.[23]

To prepare the LyP-1-modified nanoparticles, inorganic Bi_2S_3 nanoparticles were first synthesized by hot-injection of elemental sulfur into a boiling solution of bismuth acetate in 1-octadecene containing oleic acid. This procedure yielded Bi_2S_3 nanoparticles of the expected elemental composition (energy dispersive X-ray spectrum, EDS, Figure S1 in the Supporting Information), with mean diameter (by transmission electron microscopy, TEM, Figure 1 a, Figure S1c) of 10 ± 1.2 nm and with a hydrophobic oleate surface coating. The oleate-coated nanoparticles were then treated with a solution containing 1,2-diastearoyl-*sn*-glycero-3-phosphoethanolamine-*N*-[methoxy(polyethylene glycol)] (PEG_{5000}-DSPE) ($MW = 5000\ g\,mol^{-1}$) that contained a maleimide terminal group. This resulted in a noncovalent micellar overcoating on the nanoparticles. The LyP-1 peptide was then conjugated by thioether formation between the maleimide and an N-terminal cysteine moiety on LyP-1.[24–26] The resulting particle formulations had an average hydrodynamic radius of 28 nm by dynamic light scattering (DLS, Figure S1). The LyP-1 peptide-labeled Bi_2S_3 nanoparticles had no effect on the growth of cells (4T1 tumor cells or J774 macrophages;

[*] Dr. J. M. Kinsella, A. M. Rush, Prof. N. C. Gianneschi, Prof. M. J. Sailor
Department of Chemistry & Biochemistry, University of California San Diego
9500 Gilman Drive, La Jolla, CA 92093 (USA)
E-mail: msailor@ucsd.edu
R. E. Jimenez
Department of Biomedical Sciences, University of California (USA)
Dr. D. Stupack
Moores Cancer Center, University of California (USA)
Prof. M. J. Sailor
Materials Science and Engineering, University of California (USA)
Prof. M. J. Sailor
Department of Bioengineering, University of California (USA)
P. P. Karmali,[+] V. R. Kotamraju, Prof. E. Ruoslahti
Center for Nanomedicine, Sanford Burnham Medical Research Institute at University of California, Santa Barbara, 1105 Life Sciences Technology Bldg, Santa Barbara, CA 93106 (USA)
P. P. Karmali,[+] V. R. Kotamraju, Prof. E. Ruoslahti
Cancer Center Sanford Burnham Medical Research Institute
10901 N. Torrey Pines Road, La Jolla, CA 92037 (USA)
[+] Present address: Nitto Denko Technical Corporation
501 Via Del Monte, Oceanside, CA 92058 (USA)

[**] This work was supported by the National Cancer Institute of the National Institutes of Health through grant numbers U5A CA 119335 (UCsD CCNE) and 5-R01-CA124427 (Bioengineering Research Partnership). J.M.K. acknowledges support from the American Cancer Society in the form of a postdoctoral fellowship. We acknowledge use of the UCSD Cryo-Electron Microscopy Facility, which is supported in part by NIH grant 1S10 RR020016, a gift from the Agouron Institute, and UCSD funds provided to Prof. Timothy S. Baker.

Supporting information for this article is available on the WWW under http://dx.doi.org/10.1002/anie.201104507.

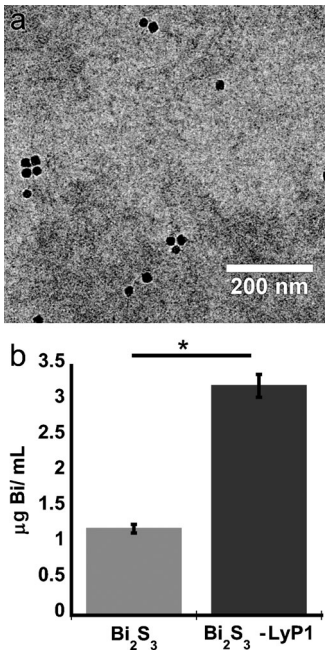

Figure 1. Physical and in vitro characterization of Bi_2S_3 nanoparticles. a) Transmission electron micrograph of Bi_2S_3 nanoparticles encapsulated in PEG_{5000}-DSPE labeled with LyP-1 peptide. b) quantity of Bi_2S_3 nanoparticles internalized by 4T1 cells in vitro, 4 h after incubation with Bi_2S_3 or LyP-1-labeled Bi_2S_3. The error bars in (b) correspond to the standard deviation calculated from at least three experiments. The asterisk in (b) corresponds to $p < 0.005$.

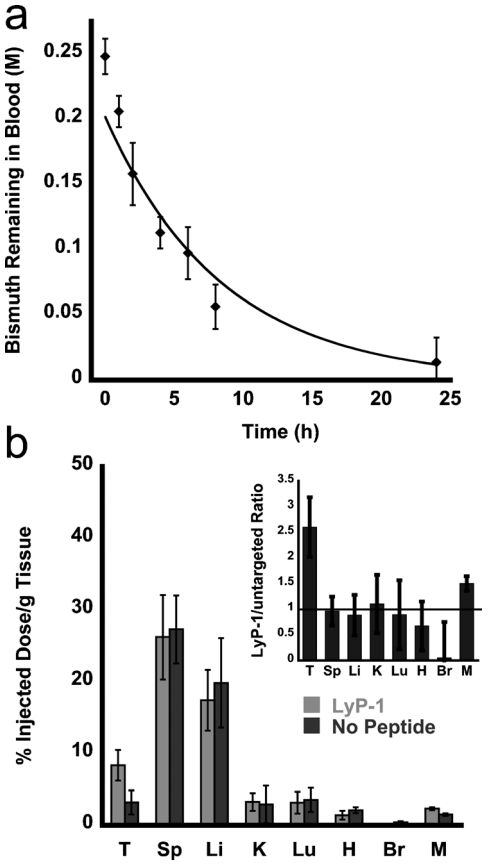

Figure 2. In vivo circulation time and biodistribution of injected Bi_2S_3 nanoparticles. a) Concentration of LyP-1-labeled nanoparticles in the blood pool of healthy female Balb/c mice as a function of time. Concentration of particles was quantified from the Bi concentration in plasma isolated from blood drawn from the suborbital space, determined by inductively coupled plasma-optical emission spectroscopy (ICP-OES). All error bars correspond to standard deviations with a sample size $n = 5$. b) Biodistribution of Bi_2S_3 nanoparticles in 4T1 tumor-burdened mice 24 h after injection as determined by ICP-OES ($n = 3$, $p = 0.03$). T = tumor, Sp = spleen, Li = liver, K = kidney, Lu = lungs, H = heart, Br = brain, M = muscle. Light gray bars (left) indicate injection of LyP-1 peptide-labeled Bi_2S_3 nanoparticles, dark gray bars (right) indicate injection with control Bi_2S_3 nanoparticles that were not labeled with peptide. The inset of (b) shows the ratio of accumulated nanoparticles that contained the Lyp-1 peptide relative to nanoparticles with no peptide attached. For all experiments in this figure, the injected dose corresponded to 200 μL of 0.25 M Bi.

Figure S2) during 24 h incubation periods at concentrations of bismuth reaching 0.5 mg mL^{-1} (2.39 mM Bi), corresponding to 19.7 μM of the LyP-1-targeting peptide (ca. 6.5 peptides per nanoparticle). The IC_{50} for the targeting peptide in its free form is ca. 66 μM.[27] The LyP-1-labeled Bi_2S_3 nanoparticles were internalized by the p32-expressing 4T1 cells with > 3-fold greater efficiency relative to non-labeled control Bi_2S_3 nanoparticles (Figure 1b). Despite the large degree of internalization, the LyP-1 peptide formulation did not induce detectable cell death at the concentrations used.

The pharmacokinetic behavior of the Bi_2S_3 nanoparticle formulation synthesized by the current method is comparable to that of the previously published Bi_2S_3 nanoparticle preparation used for microCT imaging.[12] The in vivo blood circulation half–life ($t_{1/2}$) of LyP-1-labeled Bi_2S_3 nanoparticles in healthy female Balb/c mice (intravenously injected with 200 μL doses of 0.25 M bismuth) was 230 ± 20 min, based on a single-component pharmacokinetic model (Figure 2a).

The tissue distribution of bismuth was quantified in tumor-bearing mice 24 h after injection (> 6 $t_{1/2}$), in order to allow the nanoparticle formulation sufficient time to clear from circulation (Figure 2b). The size of the nanoparticles limits renal clearance, favoring splenic and hepatic clearance mechanisms instead,[28,29] and the presence of targeting peptide exhibited no significant impact on the accumulation of the nanoparticles within these organs. Splenic uptake corresponded to 26–27% injected dose/g tissue and 17–20% injected dose/g tissue was found in the liver (Table S1). Only a small fraction of nanoparticles (approximately 4% injected dose/g tissue) were cleared renally. These renally cleared nanoparticles are proposed to possess either a smaller core radius, or to have been degraded to ionic bismuth in vivo, either of which could be expected to be more readily cleared by the kidneys. A similar proportion of Bi accumulated in the lungs, indicating that larger sized agglomerates formed during circulation. While the accumulation observed in the kidneys and lungs was small, more work is needed to determine the roles of agglomeration and degradation on the toxicity and pharmacokinetic profiles of the material. The data (Figure 2b and Table S1) show a marked increase in tumor accumulation of LyP-1-labeled nanoparticles (8.4 ± 2.1% injected dose/g tissue) relative to unlabeled nanoparticles (3.2 ± 1.7% injected dose/g tissue).

Clearance of nanoparticles from circulation was monitored in organs harvested 4 h after injection, quantified by near-IR fluorescence images of Cy7-labeled nanoparticles (Figure S3a). At this time point, clearance by the reticuloendothelial system (RES) was dominated by the liver rather than the spleen. The kidneys also showed strong fluorescence intensity, although this is likely attributable to an accumulation of Cy7-labeled polyethylene $glycol_{5000}$-DSPE molecules shed from the nanoparticle micelle during circulation. In agreement with the quantitative biodistribution data of Figure 2b, some nanoparticle accumulation was observed in the lungs. The fluorescence images indicated strong accumulation in the tumor tissues (Figure S3a). The distribution of the fluorophore appears center heavy in the spleen, liver, and tumor tissue. However, in vivo transverse microCT scans showed accumulation of nanoparticles at the tumor periphery rather than in the core of the tumor (Figure S4). The apparent discrepancy is attributed to free Cy7-labeled polyethylene $glycol_{5000}$-DSPE molecules that have been shed from the nanoparticle assembly and diffused into the tumor. The total % injected dose/gram tissue of nanoparticles in the tumor determined from the microCT data was less than in the liver or spleen (Figure S3). However, the fluorescence signal from the tumor was higher than that from the liver and spleen, indicating the accumulation of untethered Cy7-PEG500-DSPE in the core of the tumor tissue.

MicroCT images of live, tumor-bearing mice injected with Bi_2S_3 nanoparticles were acquired over a 1 day time period after injection (Figure 3 and Figure S4). The contrast agent was visualized by microCT in the vasculature immediately after injection, with subsequent scans obtained at 2, 4.5, and 24 h after injection. Consistent with the ex vivo half-life measurements (Figure 2a), the in vivo imaging data yielded $t_{1/2}$ for the nanoparticles to be ca. 4 h (Figure S7). When injected at a total Bi concentration of 0.25 M (in 200 μL injected volume), the blood pool was evident in the images (Figure S7a–d). Volume-rendered images of the mouse obtained immediately following administration showed a low degree of RES clearance into the liver and spleen, and accumulation into a small portion of the tumor. As time progressed, the RES organs became more discernible, indicative of nanoparticle accumulation. Images obtained 24 h after injection (Figure S4d, S7d) revealed significant removal of nanoparticles from the blood pool and accumulation in the liver, the spleen, and the tumor. The tumor boundaries in particular are readily visible in the data for the targeted nanoparticle (Figure 3d,f) relative to the untargeted nanoparticle (Figure S5). Quantitative analysis of the microCT contrast (in Hounsfeld units, Figure S3, S6) indicated that the tumor contained 1.7-fold more LyP-1-labeled Bi_2S_3 nanoparticles than non-labeled Bi_2S_3 nanoparticles after 4.5 h. This result is consistent with ICP-OES measurements, which indicated that twice the quantity of targeted (LyP-1-labeled) Bi_2S_3 nanoparticles accumulated in the tumor relative to unlabeled Bi_2S_3 nanoparticles (Table S2). After 7 days, LyP-1-labeled nanoparticles remained visible within the liver, spleen, and tumor tissues in the microCT images (Figure S8), indicating prolonged retention of the particles within these tissues. Notably, the intestines of the mouse also showed enhanced contrast, indicating that the nanoparticles are removed through a hepatobiliary/fecal route.

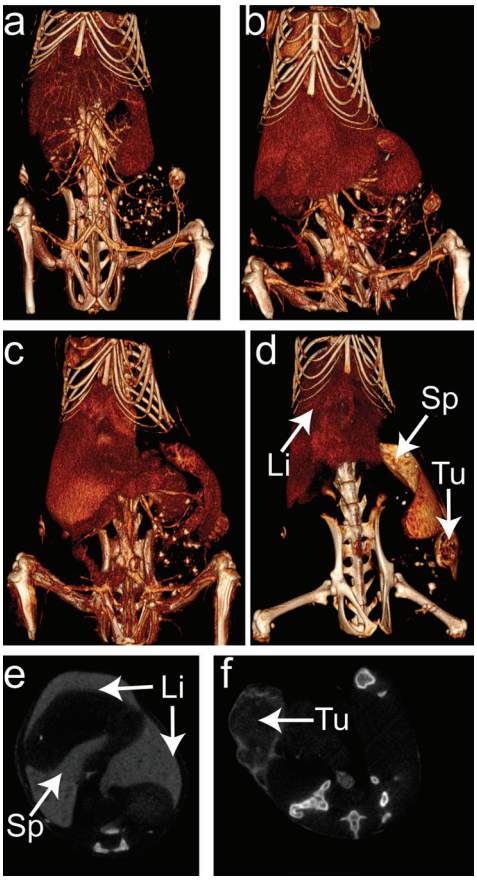

Figure 3. Micro-computed X-ray tomography images of tumor-burdened mouse injected with LyP-1-targeted Bi_2S_3 nanoparticles. a–d) Time images obtained a) immediately, b) 2 h, c) 4.5 h, and d) 24 h after injection. The window level and window width values were adjusted to show Bi_2S_3 nanoparticle accumulation in the organs and tissues. The major organs of the reticuloendothelial system (RES) and the tumor are labeled as viewing guides in (d): Li, Sp, Tu indicate the liver, spleen, and tumor, respectively. e,f) Two-dimensional transverse CT scans of e) the liver and spleen and f) tumor, obtained 24 h after injection of LyP-1-labeled Bi_2S_3 nanoparticles. The injected dose corresponded to 200 μL of 0.25 M Bi.

The data presented here are consistent with previous observations of LyP-1 peptide increasing the homing efficacy of nanoparticles to tumors that express elevated levels of the p32 cell surface receptor,[18,30–33] and it extends this theme to a new class of X-ray contrast agents, Bi_2S_3 nanoparticles. Following accumulation, the monodispersed Bi_2S_3 nanoparticles yield sufficient contrast to provide quantitative, high fidelity CT images of tumors for ca. 1 week after injection. Notably, the nanoparticles appear to undergo clearance from the mice through a fecal route during this time period. Although this limits the period of imaging, it provides a safe mechanism for nanoparticle clearance.

Received: June 29, 2011
Revised: August 26, 2011
Published online: October 26, 2011

Keywords: cancer · imaging agents · nanomedicine · nanoparticles · peptides

[1] M. Ferrari, *Nat. Rev. Cancer* **2005**, *5*, 161.
[2] A. K. Gupta, M. Gupta, *Biomaterials* **2005**, *26*, 3995.
[3] Q. A. Pankhurst, J. Connolly, S. K. Jones, J. Dobson, *J. Phys. D* **2003**, *36*, R167.
[4] X. H. Gao, Y. Y. Cui, R. M. Levenson, L. W. K. Chung, S. M. Nie, *Nat. Biotechnol.* **2004**, *22*, 969.
[5] L. R. Hirsch, R. J. Stafford, J. A. Bankson, S. R. Sershen, B. Rivera, R. E. Price, J. D. Hazle, N. J. Halas, J. L. West, *Proc. Natl. Acad. Sci. USA* **2003**, *100*, 13549.
[6] V. Kattumuri, K. Katti, S. Bhaskaran, E. J. Boote, S. W. Casteel, G. M. Fent, D. J. Robertson, M. Chandrasekhar, R. Kannan, K. V. Katti, *Small* **2007**, *3*, 333.
[7] I. L. Medintz, H. T. Uyeda, E. R. Goldman, H. Mattoussi, *Nat. Mater.* **2005**, *4*, 435.
[8] X. Michalet, F. F. Pinaud, L. A. Bentolila, J. M. Tsay, S. Doose, J. J. Li, G. Sundaresan, A. M. Wu, S. S. Gambhir, S. Weiss, *Science* **2005**, *307*, 538.
[9] Q. Y. Cai, S. H. Kim, K. S. Choi, S. Y. Kim, S. J. Byun, K. W. Kim, S. H. Park, S. K. Juhng, K. H. Yoon, *Invest. Radiol.* **2007**, *42*, 797.
[10] F. Hyafil, J. C. Cornily, J. E. Feig, R. Gordon, E. Vucic, V. Amirbekian, E. A. Fisher, V. Fuster, L. J. Feldman, Z. A. Fayad, *Nat. Med.* **2007**, *13*, 636.
[11] D. Kim, S. Park, J. H. Lee, Y. Y. Jeong, S. Jon, *J. Am. Chem. Soc.* **2007**, *129*, 7661.
[12] O. Rabin, J. M. Perez, J. Grimm, G. Wojtkiewicz, R. Weissleder, *Nat. Mater.* **2006**, *5*, 118.
[13] J. F. Hainfeld, D. N. Slatkin, T. M. Focella, H. M. Smilowitz, *Br. J. Radiol.* **2006**, *79*, 248.
[14] K. A. Miles, *Eur. J. Radiol.* **1999**, *30*, 198.
[15] S. Achilefu, R. B. Dorshow, J. E. Bugaj, R. Rajagopalan, *Invest. Radiol.* **2000**, *35*, 479.
[16] W. Arap, R. Pasqualini, E. Ruoslahti, *Science* **1998**, *279*, 377.
[17] T. Jiang, E. S. Olson, Q. T. Nguyen, M. Roy, P. A. Jennings, R. Y. Tsien, *Proc. Natl. Acad. Sci. USA* **2004**, *101*, 17867.
[18] M. E. Åkerman, W. C. W. Chan, P. Laakkonen, S. N. Bhatia, E. Ruoslahti, *Proc. Natl. Acad. Sci. USA* **2002**, *99*, 12617.
[19] A. M. Morawski, G. A. Lanza, S. A. Wickline, *Curr. Opin. Biotechnol.* **2005**, *16*, 89.
[20] E. Ruoslahti, S. N. Bhatia, M. J. Sailor, *J. Cell Biol.* **2010**, *188*, 759.
[21] P. Laakkonen, K. Porkka, J. A. Hoffman, E. Ruoslahti, *Nat. Med.* **2002**, *8*, 751.
[22] F. Zhang, G. Niu, X. Lin, O. Jacobson, Y. Ma, H. S. Eden, Y. He, G. Lu, X. Chen, *Amino Acids* **2011**, DOI: 10.1007/s00726-011-0976-1.
[23] V. Fogal, L. Zhang, S. Krajewski, E. Ruoslahti, *Cancer Res.* **2008**, *68*, 7210.
[24] H. Ai, C. Flask, B. Weinberg, X. T. Shuai, M. D. Pagel, D. Farrell, J. Duerk, J. Gao, *Adv. Mater.* **2005**, *17*, 1949.
[25] V. P. Torchilin, *Pharm. Res.* **2007**, *24*, 1.
[26] B. Dubertret, P. Skourides, D. J. Norris, V. Noireaux, A. H. Brivanlou, A. Libchaber, *Science* **2002**, *298*, 1759.
[27] P. Laakkonen, M. E. Åkerman, H. Biliran, M. Yang, F. Ferrer, T. Karpanen, R. M. Hoffman, E. Ruoslahti, *Proc. Natl. Acad. Sci. USA* **2004**, *101*, 9381.
[28] H. S. Choi, W. Liu, P. Misra, E. Tanaka, J. P. Zimmer, B. I. Ipe, M. G. Bawendi, J. V. Frangioni, *Nat. Biotechnol.* **2007**, *25*, 1165.
[29] W. H. De Jong, W. I. Hagens, P. Krystek, M. C. Burger, A. J. A. M. Sips, R. E. Geertsma, *Biomaterials* **2008**, *29*, 1912.
[30] J. H. Park, G. Von Maltzahn, M. J. Xu, V. Fogal, V. R. Kotamraju, E. Ruoslahti, S. N. Bhatia, M. J. Sailor, *Proc. Natl. Acad. Sci. USA* **2010**, *107*, 981.
[31] G. Luo, X. Yu, C. Jin, F. Yang, D. Fu, J. Long, J. Xu, C. Zhan, W. Lu, *Int. J. Pharm.* **2010**, *385*, 150.
[32] P. P. Karmali, V. R. Kotamraju, M. Kastantin, M. Black, D. Missirlis, M. Tirrell, E. Ruoslahti, *Nanomedicine* **2009**, *5*, 73.
[33] G. von Maltzahn, Y. Ren, J. H. Park, D. H. Min, V. R. Kotamraju, J. Jayakumar, V. Fogal, M. J. Sailor, E. Ruoslahti, S. N. Bhatia, *Bioconjugate Chem.* **2008**, *19*, 1570.

